photonics

MDPI

Article

Comparison of Imaging Properties of Bangerter Foils and Myopia Control Spectacle Lens †

Susanna Pearline Clement [1,*], Augusto Arias [1] and Siegfried Wahl [1,2]

[1] Institute for Ophthalmic Research, University of Tübingen, Elfriede-Aulhorn-Str. 7, 72076 Tuebingen, Germany; augusto.arias-gallego@uni-tuebingen.de (A.A.); siegfried.wahl@zeiss.com (S.W.)
[2] Carl Zeiss Vision International GmbH, Turnstrasse 27, 73430 Aalen, Germany
* Correspondence: susanna-pearline.clement@uni-tuebingen.de
† This article is a revised and expanded version of an abstract entitled "Comparison of Imaging Properties of Bangerter Foils and a Scattering-Based, Myopia-Control Spectacle Lens", which was presented at the ARVO Annual Meeting 2025.

Abstract

To evaluate whether Bangerter foils (BFs) could serve as a low-cost myopia control intervention, we measured and compared the imaging properties of fifteen BFs from two manufacturers, four myopia control spectacles, and a single-vision lens. Image quality metrics related to light-signaling theories of myopia onset and progression were evaluated in three tests: i. the assessment of the focusing properties through the maximum of the point spread function (MaxPSF), modulation transfer function (MTF), and area under the MTF (AUMTF); ii. the quantification of the scattered light (s) using the optical integration method; and iii. the calculation of the Michelson contrast (MiC) on a binary grating imaged under dark and bright illumination. BFs exhibited lower MaxPSF, AUMTF, and MTF values than the myopia control lenses. Except for one 0.6-graded BF, none of the other BFs mimicked the scattering behavior of the diffusion optics technology lenses. Moreover, BFs showed lower MiC values than with myopia control lenses under both lighting conditions. Although the BFs did not replicate the imaging properties of myopia control lenses, they still demonstrated effective contrast reduction across the lighting conditions. Whether they may help to slow myopia progression remains uncertain, perhaps even unlikely, given the fundamental imaging differences.

Keywords: myopia control lenses; Bangerter foils; imaging properties

1. Introduction

Myopia, or shortsightedness, is a refractive condition in which an unaccommodated eye focuses light rays in front of the fovea, resulting in blurred images [1].The standard correction for myopia consists of using a negative lens to sharpen the images projected onto the central retina. However, this approach is not efficient for treating the progression of myopia, which leads to excessive eye elongation, increasing the risk of secondary ocular diseases (e.g., glaucoma and retinal detachment) [2]. Over the last decade, multiple interventions to control myopia progression have been developed, involving light therapies [3,4], pharmaceutical agents [5], Ortho-k lenses [6,7], and specialized ophthalmic lenses. These ophthalmic lenses can induce peripheral defocus [8–10] or reduce the contrast in the peripheral retina [11].

Most of the current myopia management lenses are based on the simultaneous competing defocus theory [8–10], incorporating arrays of positive lenslets. According to this theory,

Received: 23 January 2026
Revised: 20 February 2026
Accepted: 26 February 2026
Published: 4 March 2026

the axial elongation of the eye can be slowed or reversed by projecting sharp images in front of the peripheral retina. However, an alternative theory suggests that the effect of the optical structures in myopia control lenses is filtering out high spatial frequencies, which can have an impact on reducing myopia progression [12]. This concept is supported by the fact that the emmetropization process depends mainly on the peripheral retina (around 6–10° from the fovea) [13,14] and primarily relies on spatial frequencies between 3 and 4 cpd [14]. A third theory ('contrast theory') posits that reducing the contrast across all spatial frequencies in the peripheral retina mitigates the abnormal contrast signaling of certain cones [15]. This abnormal response might originate from a set of haplotypes that affects the efficiency of those cones in absorbing light, thereby accelerating the axial elongation of the eye. Currently, only one spectacle lens, known as the 'Diffusion Optics Technology' (DOT) lens, is based on this theory. This lens incorporates an array of micro-diffusers to scatter the light in order to reduce the contrast of the images in the retina without blurring them. Recent clinical studies comparing the refractive error, axial length, and choroidal thickness changes in children wearing lenses based on simultaneous competing defocus [8–10] and contrast [15] theories demonstrated a slower myopia progression compared to the children who wore standard single-vision lenses.

Given the role of peripheral retinal contrast reduction and blur in myopia management, Bangerter foils (BFs) may represent a relevant myopia control intervention. BFs reduce contrast sensitivity and visual acuity by incorporating arrays of microstructures that act as low-pass filters [16] and increase the amount of scattered light [17]. BFs are available in various grades (0.1–1.0 and 'Light perception'), with the nominal grade corresponding to the expected visual acuity reduction. BFs have been widely used in the treatment of amblyopia; however, a recent study [18] showed that non-amblyopic eyes occluded with low-graded BFs exhibited slow axial elongation, suggesting the potential application of BFs for myopia control. This possible use would offer a simple means of converting a standard single-vision lens into a cost-effective, non-invasive treatment modality. Before proceeding to clinical trials to determine the efficacy of BFs in slowing down myopia progression, a logical step is to compare the imaging properties of BFs with those of existing myopia control lenses, whose optical characteristics have been assessed to investigate their underlying mechanisms [19–22].

In this study, we comprehensively characterize and compare the imaging properties of myopia control lenses and BFs within a common framework to determine whether BFs replicate the imaging characteristics of myopia control lenses. These properties encompass both focusing and scattering properties. While the former primarily refers to the sharpness and contrast of images formed on the retina under scotopic and mesopic conditions, the latter accounts for contrast reduction under photopic illumination. Both sharpness and contrast are directly linked to light-signaling theories implicated in myopia onset and progression that underpin current optical interventions, as described above. Therefore, in this study, we characterize and compare the imaging properties of myopia control lenses and BFs within a common framework to determine whether BFs replicate the imaging characteristics of myopia control lenses, a crucial step in evaluating the potential of BFs for myopia control. Our characterization is based on the peak intensity of the image of a point source (or point spread function, PSF), the modulation transfer function (MTF), the contrast under different lighting conditions, and the amount of scattered light.

2. Methodology

2.1. Tested Samples

The image properties of a total of 20 samples were tested, which include:

- Four myopia control lenses: two Diffusion Optical Technology (DOT) lenses from SightGlass Vision Inc. (Palo Alto, CA, USA) and Nikon (Beijing, China); one Defocus Incorporated Multiple Segment (DIMS) lens from Hoya Corporation (Tokyo, Japan), and one Stellest lens from Essilor (Charenton-Le-Pont, France). While DIMS and Stellest are based on the simultaneous competing defocus theory, DOT lenses are based on the contrast theory. Table 1 lists the nominal optical parameters of these lenses.
- Fifteen BFs: 8 from Ryser Optik AG (RO; St. Gallen, Switzerland), graded 1.0, 0.8, 0.6, 0.4, 0.3, 0.2, 0.1, and light perception (LP); and 7 from Breitfeld & Schliekert GmbH (BS; Karben, Germany), graded 0.8, 0.6, 0.4, 0.3, 0.2, 0.1, and light perception (LP). These BFs were adhered to a plano flat lens to test their properties.
- A single-vision lens with a base power of −2D, serving as a reference (Carl ZEISS Vision International GmbH, Aalen, Germany).

Table 1. Nominal optical parameters of the tested spectacle lenses. The characteristics of the peripheral structures of the DIMS and Stellest lenses were taken from [8,10], respectively.

	DOT SightGlass	DOT Nikon	DIMS	Stellest	Single Vision
Base power			−2 D		
Material	Trivex	Plastic	Polycarbonate	Polycarbonate	CR39
Size of the clear zone	5 mm	5 mm	9 mm	9 mm	-
Type of peripheral structures	Micro-diffusers	Micro-diffusers	Spherical lenslets (size, 1.03 mm)	Aspherical lenslets (size, 1.1 mm)	-
Arrangement of peripheral structures	Square	Square	Hexagonal (period, 1.5 mm)	Annular rings (period, 2.3 mm)	-

DOT lenses and BFs contain micro-diffusers that were imaged, and their spatial characteristics and distributions were measured using ImageJ (version 1.54g; National Institutes of Health, Bethesda, MD, USA).

2.2. Measurement of the Focusing Properties

The focusing properties of samples were evaluated through the PSFs over a narrow angular domain, using an in-house instrument introduced in [20]. This instrument, shown in Figure 1, consists of a green (wavelength, 532 nm) collimated laser beam illuminating the samples under testing at two eccentricities (0° and 20°). The light passes through the samples towards a steering mirror, located 20 mm behind the sample, which directs the beam to a liquid crystal spatial light modulator (SLM; LETO, Holoeye Photonics AG, Berlin, Germany). The SLM, optically conjugated to the mirror by a first telescope, is used to compensate for the aberrations of the setup without samples; shape the pupil as a disk with a diameter of 5 mm; and acquire the through-focus PSF (TF-PSF) by adding programmed amounts of defocus. Such defocus is calculated as $(\pi/\lambda)D_{add}r^2$, where λ is the wavelength, r is the radial coordinate at the pupil plane, and D_{add} is the amount of defocus. Pupil shaping is implemented by superimposing a binary grating (period, 12.8 μm; depth, π radians) onto the phase maps displayed on the SLM within the pupil area and filtering the first-order diffraction generated by this grating using field stop in the second telescope. Further details about the phase maps displayed on the SLM are explained elsewhere [19]. A second telescope optically conjugates the SLM with a focusing lens, which projects in- and out-of-focus PSFs over the camera (DMK23UM021, The Imaging Source GmbH, Bremen, Germany) for their acquisition. The telescopes for conjugating the steering mirror, SLM, and focusing lens incorporated field stops to restrict the width of the PSFs up to 1.9 degrees. The second telescope also incorporates a rotational linear polarizer (RLP) to

modulate the PSF peak, preventing saturation or underexposure of the captured PSF. This functionality is based on Malus's Law and the fact that the light modulated by the SLM is horizontally polarized.

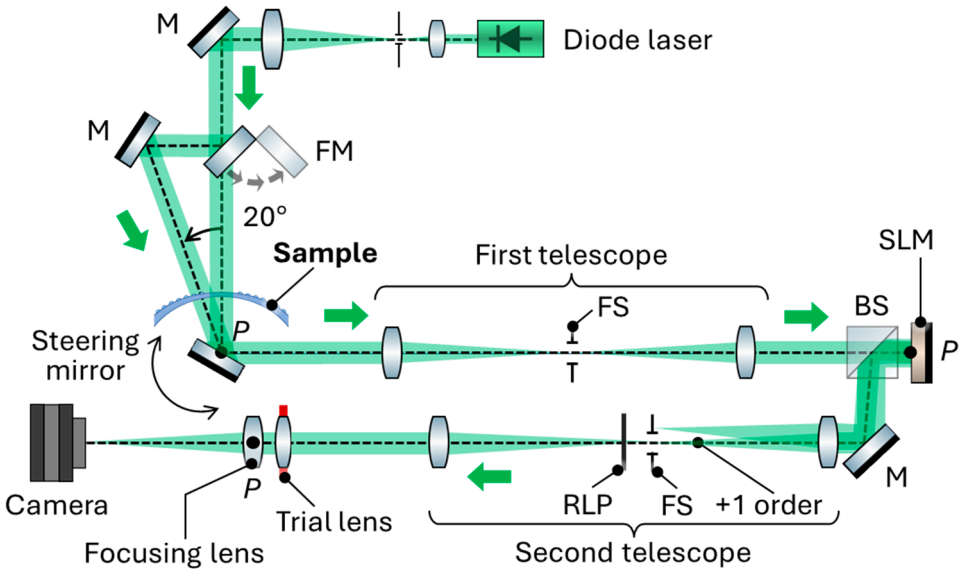

Figure 1. In-house instrument for measuring the focusing properties of the samples. A collimated beam illuminates the samples at 0° and 20° eccentricities, selectable via a foldable mirror (FM). The pupil plane (P), located behind the sample at a steering mirror, is relayed by a first telescope onto a spatial light modulator (SLM), where spherical and binary phase patterns introduce programmable defocus and shape the pupil amplitude, respectively. A field stop (FS) in a second telescope blocks the zero-diffraction order, enabling the reproduction of the shaped pupil on a focusing lens that images the point spread function (PSF) onto a camera. This telescope also incorporates a trial lens to compensate for the base power of the tested spectacle lenses, and a rotational linear polarizer (RLP) to adjust the PSF peak intensity. M, mirror; BS, beam splitter.

Three image quality descriptors were assessed from the acquired PSFs: the maximum of the PSF (max PSF), the modulation transfer function (MTF), and the area under the MTF (AUMTF) up to 60 cycles per degree (cpd). The MTF was computed by applying the fast Fourier transform to the PSF. The AUMTF was calculated as:

$$AUMTF = \sum_{j=1}^{M}\sum_{i=1}^{M} circ(i,j)MTF_{i,j}\left(\Delta f^2\right) \quad (1)$$

where $MTF_{i,j}$ is the element (i,j) of the $M \times M$ matrix that contains the MTF values, $circ(i,j)$ is a function valued 1 for $\Delta f\sqrt{i^2+j^2} \leq 60$ cpd and 0 otherwise, and Δf is the pixel size of the MTF matrix in spatial frequency units. In this study, Δf was set to approximately 0.4 cpd. The reported maximum of the PSF and AUMTF were normalized to their corresponding values for the instrument without sample and with the aberrations corrected.

Once the aberrations of the instrument were assessed and corrected, the samples were tested through the following procedures. For myopia control lenses: i. the lens was positioned in front of the steering mirror and centered with respect to the beam with an eccentricity of 0°; ii. a trial lens was positioned in front of the focusing lens to compensate for the base power of the lens under testing; iii. PSF through the central zone was finely focused on the camera using the SLM; iv. the eccentricity of the illumination was switched to 20°; and v. the PSFs were acquired for programmed amounts of defocus between −5 and 5 D. For BFs, i. a clear, plano lens is positioned in front of the steering mirror; ii. the PSF through the plano lens at 20° of eccentricity was refocused using the SLM; ii. the plano

lens was taken out, the BF was adhered to it, and repositioned the lens in front of the steering mirror; and iii. PSFs were acquired for programmed amounts of defocus between −5 and 5 D. For each myopia control lens and BF, this procedure was repeated three times to report the mean values of MaxPSF, MTFs, and AUMTFs. In each repetition at 20°, the samples were slightly shifted in the transversal direction to measure the effect of different topographic patterns.

2.3. Measurement of the Amount of Scattered Light

The optical integration method [20] was used to quantify the amount of scattered light generated by the samples. Figure 2 shows the custom-made setup for implementing this method. The setup consists of a monitor in front of the sample under test and an artificial eye. The artificial eye is composed of a convergent lens with an attached pupil (diameter of 5 mm) and a camera. The distance between the convergent lens and the camera was adjusted to sharpen the images. The samples are located right in front of the artificial eye's pupil. All the samples were measured in a dark room.

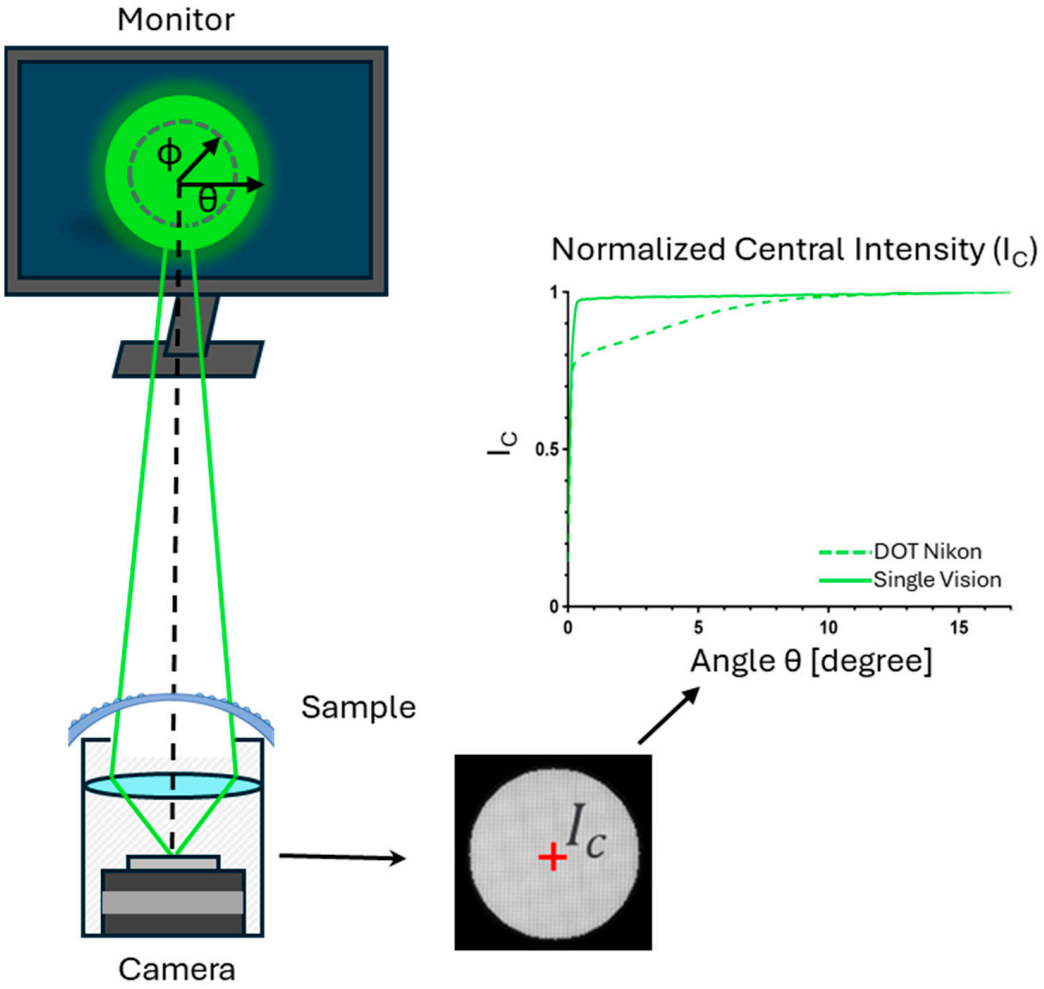

Figure 2. Custom-made setup for quantifying the amount of scattered light in the tested samples. Disks with varying angular radius (θ) are displayed on a monitor, projected through the sample, and imaged onto the camera of an artificial eye. For each θ, the central intensity (Ic) is recorded. The red plus in the figure indicates the center of the disk. All point sources within a disk contribute to Ic, with an intensity proportional to the point spread function (PSF) evaluated at the distance ϕ from the center, as indicated by Equation (2). As examples, Ic is shown as a function of θ for single-vision and DOT Nikon lenses. The PSF as a function of θ, PSF(θ), is calculated from the Ic and θ data using Equation (3), and scattered light is quantified as $\theta^2 \times$ PSF(θ), with θ in degrees.

For each sample, the amount of light scattered at an angle (θ) was measured at three different positions and subsequently averaged. For each position, the measurements consist of projecting disks with a varying angular radius θ on the monitor capturing their images through the sample. The central intensity (Ic) of each disk is related to the PSF:

$$\mathrm{Ic}(\theta) = \int_0^{\theta} \mathrm{PSF}(F) 2\pi F \, \mathrm{d}F \tag{2}$$

where F is the radial coordinate at the image plane. This formula indicates that Ic is the sum of the contributions from all bright points within the disk with a value given by PSF(F).

Then, the PSF is derived from Ic by:

$$\mathrm{PSF}(\theta) = \frac{1}{2\pi\theta} \frac{\mathrm{dIc}(\theta)}{\mathrm{d}\theta} \tag{3}$$

The derivative in Equation (3) was computed by evaluating the slopes of Ic data as a function of θ. Moreover, Ic was normalized to the value at the maximum angle (i.e., θ = 17°), allowing for reporting PSF in units of inverse stereoradian (sr−1).

Lastly, the scattering parameter (s), which quantifies the amount of scattered light at every angle θ, was defined as:

$$\mathrm{s}(\theta) = \theta^2 \times \mathrm{PSF}(\theta) \tag{4}$$

where θ is in degrees (deg). Hence, the units of s are deg2sr−1.

2.4. Measurement of the Luminance Dependence of Contrast

Figure 3 shows the setup to measure the luminance dependence of contrast of the samples. This setup consists of a monitor located in front of the sample under test, and the sample placed at 13 mm in front of an artificial eye. The artificial eye incorporates a pupil (diameter of 5 mm), a convergent lens, and a camera, as used in Section 2.3. A binary grating, with a period of 5 cpd and size of 1.5 degrees, was projected on the monitor. This grating was imaged through the BFs, the single-vision lens, and the peripheral structures of myopia control lenses. The camera was moved axially to refocus the image of the grating. The contrast of the grating was quantified through the Michelson contrast (MiC), calculated by:

$$\mathrm{MiC} = \frac{L_{max} - L_{min}}{L_{max} + L_{min}} \tag{5}$$

where L_{max} and L_{min} are the maximum and minimum intensities, respectively.

MiC was calculated under two different lighting conditions: (i) dark, referring to a dark room with a dark background projected in the monitor, and (ii) bright, referring to a bright room (using a light ring) with a dark background. The luminance at the pupil plane of the artificial eye was measured with a light meter (HS1010, China), with readings of 0 and ~850 Lux for the dark and bright conditions, respectively.

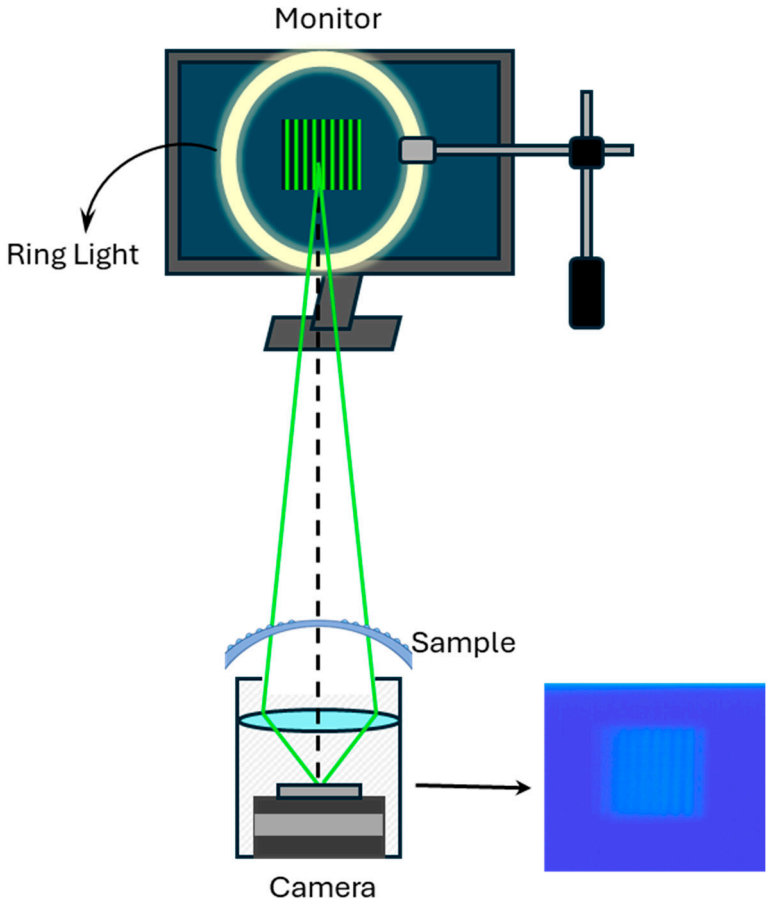

Figure 3. Setup for measuring the Michelson contrast of binary gratings imaged through the samples under controlled lighting conditions generated by a ring light.

3. Results

3.1. Microscopic Images

Figure 4 shows the microscopic images (magnification, 10×) of the BFs and the periphery of DOT lenses. From these images, the size and periodicity of the observed microstructures were measured and are listed in Table 2. BFs with the same grade but from different manufacturers exhibited microstructures that differed in periodicity, size, and shape. For example, microstructures in BFs from Ryser Optik are larger than those in BFs from Breitfeld & Schliekert. Additionally, the patterns in BFs from Ryser Optik appear more regular and evenly spaced, whereas the microstructures in BFs from Breitfeld & Schliekert are irregular. Such differences suggest distinct focusing and scattering properties. In contrast, the two DOT lenses exhibited micro-diffusers of a similar size; however, the etched internal patterns indicate different manufacturing processes.

3.2. Focusing Properties

Figure 5 shows the calculated image quality metrics related to the focusing properties. Figure 5a,b show MaxPSF and AUMTF, respectively, of the samples tested as a function of the added defocus. Positive and negative added defocuses correspond to myopic and hyperopic blur, respectively. Or, in other words, positive and negative added defocuses correspond to positions behind and in front of the detector relative to its nominal position (i.e., zero added defocus), respectively. According to these results, except for BFs graded as "Light perception", most of the samples maximize both MaxPSF and AUMT at zero defocus. In general, BFs led to poorer image quality than the myopia control lenses at zero defocus. Moreover, at this defocus value, BFs from the same manufacturer did not

consistently decrease MaxPSF and AUMTF with their grade. For instance, the 0.2-graded BF from Breitfeld & Schliekert exhibited a higher MaxPSF and AUMTF than the 0.3-graded BF, and, similarly, MaxPSF was higher in the 0.1-graded BF from Ryser Optik than the 0.2-graded BF.

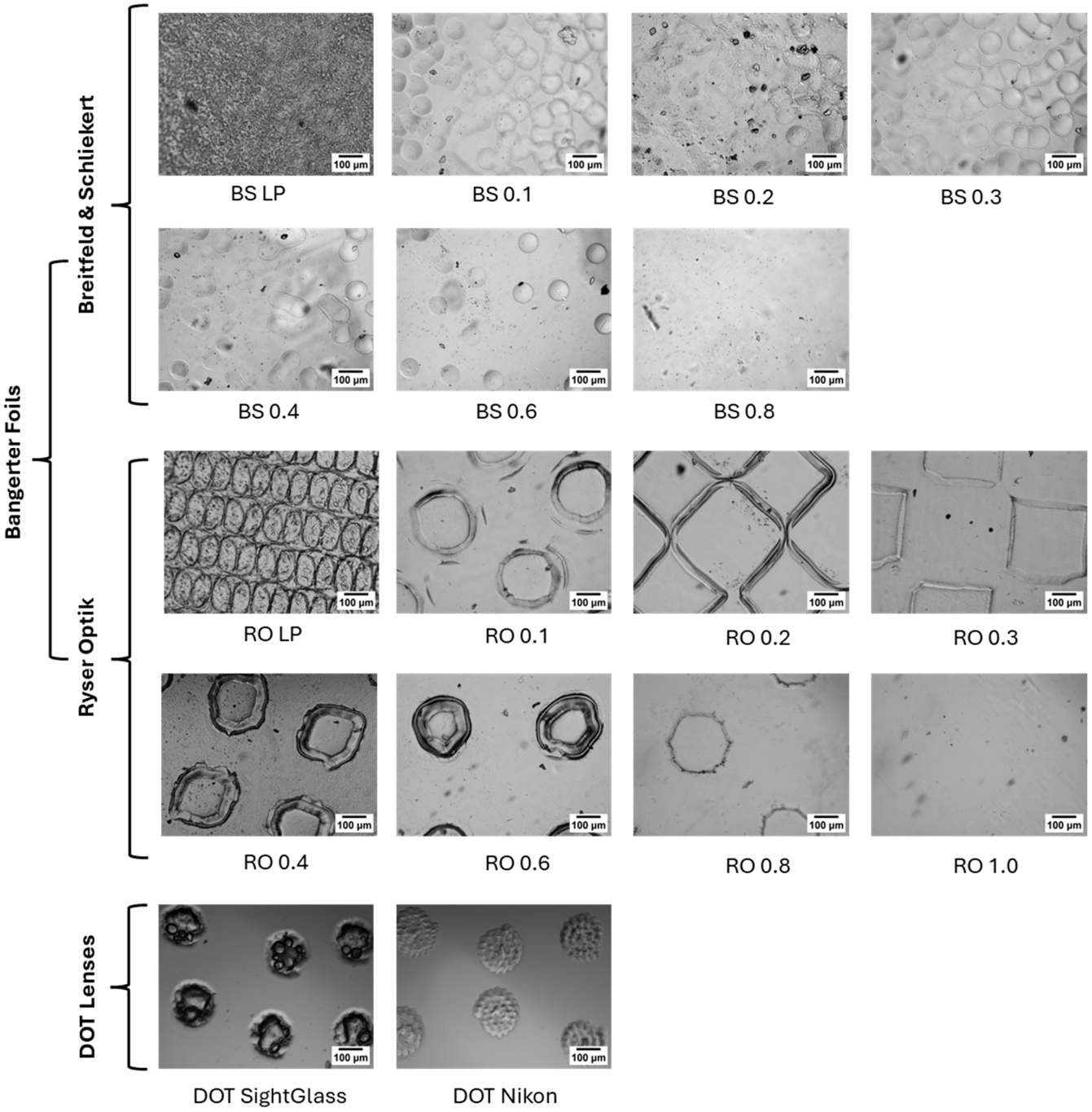

Figure 4. Microscopic images of the tested BFs from Breitfeld & Schliekert (BS) and Ryser Optik (RO) and Diffusion Optical Technology (DOT) lenses with a 10× magnification.

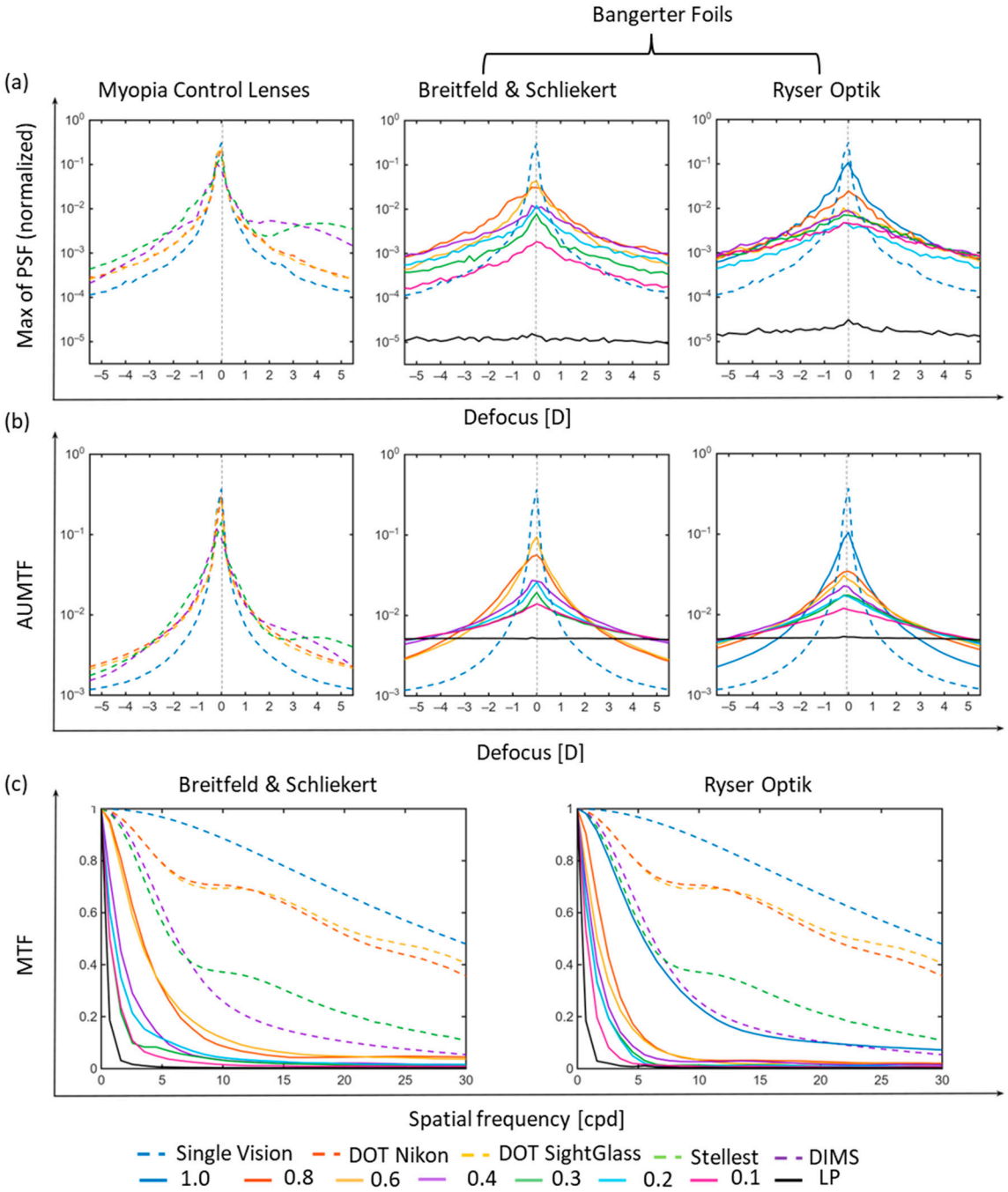

Figure 5. Image quality descriptors of the Bangerter foils and myopia control lenses, derived from the point spread functions (PSF) acquired with the instrument shown in Figure 1. (**a**) Maximum intensity of the PSF (MaxPSF) as a function of the added defocus. (**b**) Area under the modulation transfer function (AUMTF) as a function of the added defocus. (**c**) Modulation transfer function (MTF) up to 30 cycles per degree (cpd) with no added defocus. In panels (**a**,**b**), positive and negative defocus values correspond to positions behind and in front of the detector relative to its nominal position (i.e., zero added defocus), respectively.

Figure 5c shows the MTF values as a function of the spatial frequency at zero defocus for the tested samples. MTFs of BFs from both manufacturers with grades lower than 1.0 led to lower MTF values than myopia control lenses. The MTF values of the 0.1-graded BF from Ryser Optik and the DIMS lens were similar.

Table 2. Morphological parameters of the microstructures in the Bangerter foils (BF) and Diffusion Optical Technology (DOT) lenses. * BF from Breitfeld & Schliekert with light perception (LP) grade contains structural features spanning a wide range of sizes, with a median feature size of approximately 15 µm.

Parameters of Microstructures	Sample							
	DOT lenses							
	SightGlass					Nikon		
Size (µm)	140–170					150–200		
Periodicity (µm)	300–550					250–550		
	Bangerter foils from Breitfeld & Schliekert (BS)							
	BS 0.8	BS 0.6	BS 0.4	BS 0.3	BS 0.2	BS 0.1	BS LP	
Size (µm)	-	80–82	75–220	80–150	90–160	80–170	15 *	
Periodicity (µm)	-	150–500	150–300	130–200	150–170	80–200	*	
	Bangerter foils from Ryser Optik (RO)							
	RO 1.0	RO 0.8	RO 0.6	RO 0.4	RO 0.3	RO 0.2	RO 0.1	RO LP
Size (µm)	-	200–250	230–300	230–300	400–450	350–400	200–250	80–170
Periodicity (µm)	-	550–600	500–550	400–450	500–550	450–500	400–450	80–100

3.3. Amount of Scattered Light

Figure 6 shows the angular distribution of the scattering parameter (s) for the tested samples. Both DOT lenses show similar maximum amounts of scattered light, albeit at different angles: DOT SightGlass reached 68.25 deg^2/sr at 9 degrees, whereas DOT Nikon peaked at 68.95 deg^2/sr at 5 degrees. Among the BFs, only the 0.6-grade from Ryser Optik (yellow line in Figure 6b) showed an angular dependence of s similar to that of one of the DOT lenses, the DOT SightGlass (dotted yellow line in Figure 6b). The angular dependence of s was consistent between the two manufacturers only for the light perception grade; for other grades, clear inter-manufacturer differences were observed. Specifically, BFs from Breitfeld & Schliekert with grades ≤ 0.6 exhibited sharp distributions of s with peaks between 1° and 4°, while BFs from Ryser Optik with grades ≤ 0.8 spread and lowered s over wider angular ranges. In contrast, 1.0-grade BF from Ryser Optik and 0.8-grade BF from Breitfeld & Schliekert did not produce measurable additional scattered light beyond the baseline contribution of the measurement setup.

3.4. Luminance Dependence of Contrast

Figure 7 shows the Michelson contrast (MiC) measured through the samples under dark and bright lighting conditions, along with the relative MiC reduction from dark to bright. The values for BFs with a light perception grade cannot be evaluated due to the poor quality of the imaged grating. Under dark conditions, the two DOT lenses exhibited similar MiCs, and the MiC measured through the BFs from both manufacturers was notably lower than that through myopia control lenses. These results are consistent with the MTF values show in Figure 5c. On the other hand, under bright conditions, the DOT SightGlass showed lower MiC than DOT Nikon, and BFs with grades < 0.8 yielded a lower MiC than the DOT lenses. Moreover, the relative MiC reduction notably differed between BFs with the same grade but different manufacturers. These findings can be attributed to the differences in the magnitude and distribution of scattered light in the DOT lenses and BFs (see Figure 6), which directly influence the contrast degradation under increased illumination.

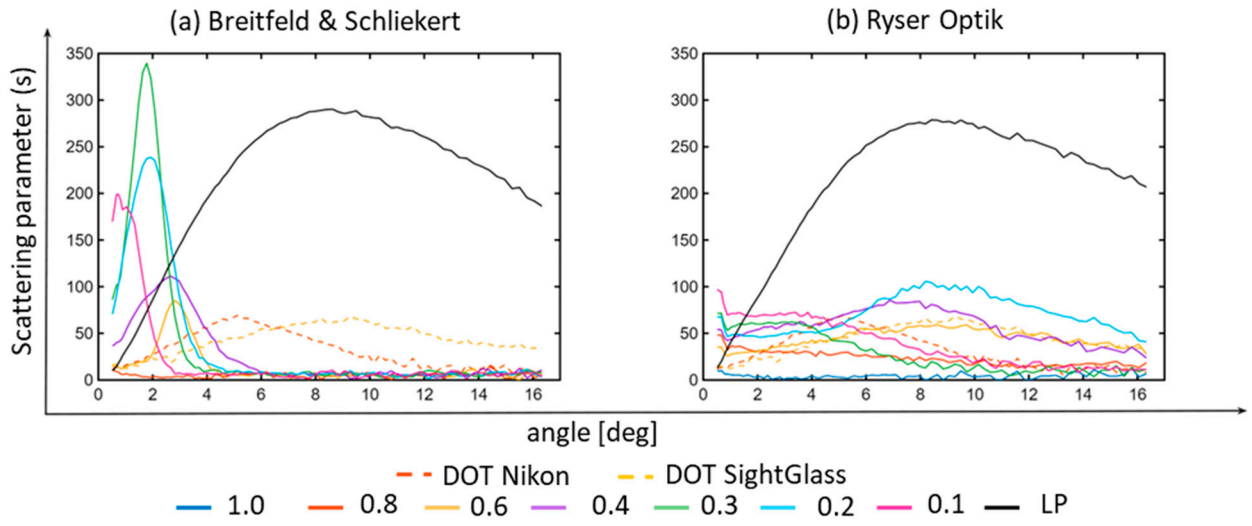

Figure 6. Angular dependence of the scattering parameter s (in units of deg^2/sr^{-1}), which quantifies the amount of light scattered by the Bangerter foils from (**a**) Breitfeld & Schliekert and (**b**) Ryser Optik, as well as by the two DOT lenses. This quantification was performed using the optical integration method implemented in the setup shown in Figure 2.

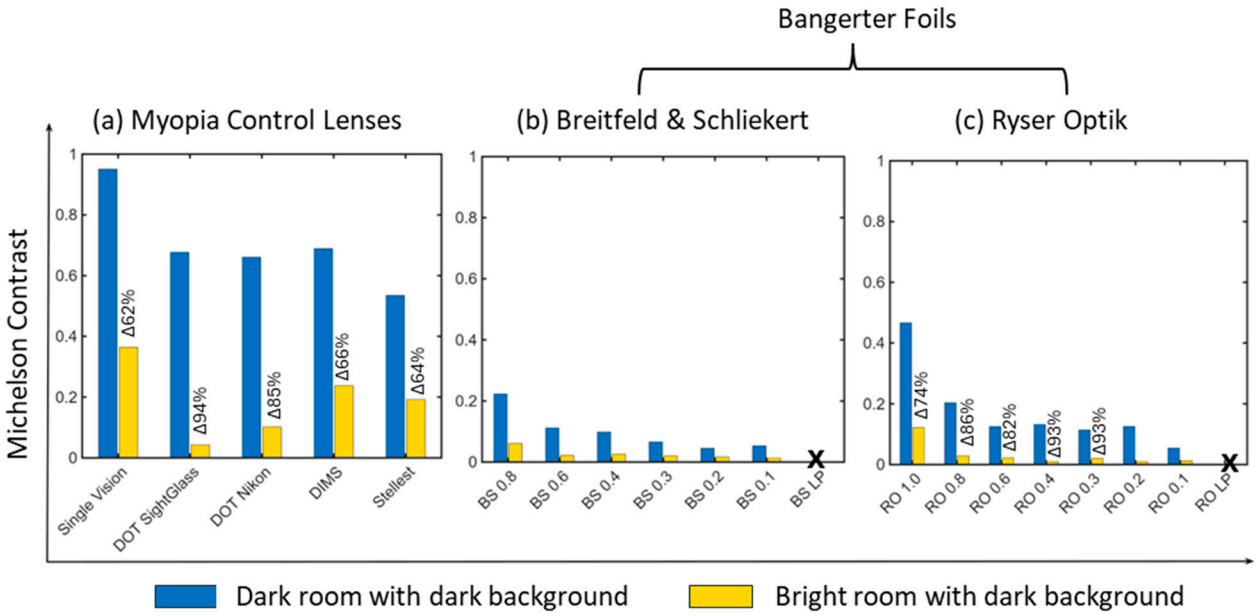

Figure 7. Michelson contrast under dark and bright lighting conditions, measured through (**a**) myopia control lenses, (**b**) Bangerter foils (BFs) from Breitfeld & Schliekert (BS), and (**c**) BFs from Ryser Optik (RO). Δ values (in percentage) represent the relative reduction in contrast from dark to bright conditions. The missing Michelson contrast for BFs graded LP is marked with an "X" in (**b**,**c**).

4. Discussion

The present study determines whether Bangerter foils can mimic the imaging properties of myopia control lenses based on the contrast (DOT lenses from SightGlass and Nikon) and simultaneous competing blur (DIMS and Stellest) theories. Our analysis is based on the assessment of: (i) the image quality metrics (MaxPSF, MTF, and AUMTF) derived from the point spread function, (ii) the angular dependence of the scattered light, and (iii) the Michelson contrast of a binary grating under dark and bright lighting conditions. The results showed that BFs failed to replicate the imaging properties of the myopia control lenses. In comparison with DIMS and Stellest lenses, BFs did not provide multifocality

and exhibited poorer image quality. In general, the amount and angular dependence of the scattered light differed among the BFs and the myopia control lenses. Similar to the DOT lenses, the Michelson contrast measured through BFs strongly depends on the lighting condition; however, BFs led to lower contrast than these lenses. These findings are discussed below.

Regarding the focusing properties, BFs led to poorer image quality than the tested myopia control lenses across all spatial frequencies. For example, the MaxPSF and AUMTF of the BFs from both Ryser Optik and Breitfeld & Schliekert across all grades were lower than myopia control and single-vision lenses at zero defocus. However, while MaxPSF and AUMTF values dropped rapidly as the defocus increased in myopia control and single-vision lenses, BFs showed a comparatively slower decline, showing that the image quality for BFs is less affected by a varying defocus.

Regarding the scattering properties, DOT lenses and BFs from both manufacturers exhibited high amounts of scattered light. However, the angular distribution of these amounts differs among the BFs and DOT lenses (see Figure 4) due to differences in the morphology and distribution of their microstructures, as shown in Table 2. Exceptionally, a 0.6-graded BF from Ryser Optik showed a similar angular distribution of scattered light to that of DOT SightGlass. These quantified amounts of scattered light were manifested as a decrease in the Michelson contrast (MiC) of a grating imaged through the BFs and peripheral structures of myopia control lenses under bright illumination relative to dark room conditions. Among the myopia control lenses, the DOT lenses led to a higher MiC decrease (94% and 85% for DOT SightGlass and Nikon, respectively), demonstrating that those lenses are more effective in reducing the spatial contrast under photopic conditions. In general, the BFs caused greater decreases in MiC than the lenses incorporating lenslets, with the BFs from Ryser Optik producing a larger MiC reduction than those from Breitfeld & Schliekert.

Although the BFs did not replicate the imaging properties of the tested myopia control lenses, this does not imply that they would be ineffective in slowing myopia progression. According to contrast theory, which underpins the design of DOT lenses, myopia progression can be mitigated by reducing the contrast of images projected onto the peripheral retina. Our results indicate that BFs reduce image contrast more effectively than DOT lenses, as BFs lower contrast under both mesopic and photopic lighting conditions, whereas the contrast reduction produced by DOT lenses is effective only under photopic conditions.

It is important to note that the imaging properties of the tested BFs were not consistently related to their grade. This observation aligns with previous studies that have characterized the optical performance and visual function of BFs [16,23]. In addition, the distribution of microstructures on the surface of the BFs was not uniform. We therefore anticipate that such manufacturing inconsistencies could lead to variations in optical properties, even among foils of the same grade and manufacturer. As a result, a limitation of our study is that the present characterizations cannot be generalized to all foils from the same manufacturers or grades, despite measurements being performed at three different locations on each BF.

Given the association between myopia (and its progression) and the changes in ocular axial length [2], we analyzed the previously reported effects of BFs on axial elongation in humans and animals. A recent amblyopia treatment study [18] compared the changes in axial length in two groups of non-amblyopic eyes over a 10-month period. In the first group, eyes were treated with conventional patching for 2–4 h per day. In the second group, eyes were occluded full-time using BFs (0.8 and 0.6-graded) from Ryser Optik. The results demonstrated greater axial elongation in the conventionally patched group (0.29 ± 1.26 mm) compared with the BF group (0.09 ± 1.49 mm). Notably, the mean axial

elongation observed in the BF group is comparable to the values reported for established myopia control lenses over a 12-month period, including: DIMS lenses, 0.11 ± 0.02 mm [8]; DOT SightGlass, 0.15 ± 0.15 mm [11]; and Stellest, 0.13 ± 0.02 [10]. Although direct comparisons are limited by differences in age and central refractive error across the studies' populations, the similarity in mean axial elongation suggests that BFs could be used for myopia control. However, other studies evaluated the short- and long-term effects of BFs with stronger grades (i.e., 0.2, 0.1, <0.1, and light perception-graded) on humans and animals, reporting axial elongation and form deprivation myopia [24–26]. The divergent outcomes among these studies indicate that the BF grade can influence the rate of axial elongation. It is important to point out that, in all these studies, both the central and peripheral retinal fields were exposed to the optical effects of BFs. Nevertheless, to rigorously prove the efficacy of BFs as a myopia control strategy, it is essential to investigate the impact of BF-induced peripheral retinal stimulation while preserving clear central vision, thereby replicating the optical configuration of contemporary myopia control lenses. If proven effective, BFs could offer a cost-efficient and practical means of converting standard single-vision lenses into functional myopia progression treatment.

5. Conclusions

Though BFs showed scattering and contrast reduction, they are inconsistent in replicating the property of myopia control lenses. Importantly, BFs are not a standard ophthalmic product, as evidenced by the differences in their microstructure morphology, focusing, and scattering properties in relation to different manufacturers. This lack of standardization could affect the reliability of a possible BF-based treatment for myopia control.

Author Contributions: Conceptualization, S.P.C., A.A. and S.W.; Methodology, S.P.C. and A.A.; Investigation, S.P.C. and A.A.; Writing—Original Draft Preparation, S.P.C.; Writing—Review and Editing, S.P.C., A.A. and S.W.; Visualization, S.P.C. and A.A.; Supervision, S.W. All authors have read and agreed to the published version of the manuscript.

Funding: Funding was received from Eberhard-Karls-University Tuebingen (ZUK 63) as part of the German Excellence initiative from the Federal Ministry of Education and Research (BMBF).

Data Availability Statement: The original contributions presented in this study are included in the article. Further inquiries can be directed to the corresponding author.

Conflicts of Interest: Author Siegfried Wahl is an employee of Carl Zeiss Vision International GmbH. All the authors declare no conflicts of interest.

Disclosures: SC: None; AA: None; SW: Carl Zeiss Vision International GmbH (E).

References

1. Saw, S.M.; Katz, J.; Schein, O.D.; Chew, S.J.; Chan, T.K. Epidemiology of myopia. *Epidemiol. Rev.* **1996**, *18*, 175–187. [CrossRef] [PubMed]
2. Smith, M.J.; Walline, J.J. Controlling myopia progression in children and adolescents. *Adolesc. Health Med. Ther.* **2015**, *6*, 133–140. [PubMed]
3. Xuan, M.; Zhu, Z.; Jiang, Y.; Wang, W.; Zhang, J.; Xiong, R.; Shi, D.; Bulloch, G.B.; Zeng, J.; He, M. Longitudinal Changes in Choroidal Structure Following Repeated Low-Level Red-Light Therapy for Myopia Control: Secondary Analysis of a Randomized Controlled Trial. *Asia-Pac. J. Ophthalmol.* **2023**, *12*, 377–383. [CrossRef] [PubMed]
4. Wang, Y.; Li, X.; Abudukeyimu, K.; Du, W.; Ning, Y.; Qi, X.; Hua, N.; Wei, N.; Ding, G.; Li, J.; et al. Low-Power Red Laser Treatment for Anisometropic Myopia Control in Children: A Contralateral Comparison Study. *Discov. Med.* **2023**, *35*, 11. [CrossRef]
5. Chua, W.-H.; Balakrishnan, V.; Chan, Y.-H.; Tong, L.; Ling, Y.; Quah, B.-L.; Tan, D. Atropine for the Treatment of Childhood Myopia. *Ophthalmology* **2006**, *113*, 2285–2291. [CrossRef]
6. Charm, J.; Cho, P. High myopia–partial reduction ortho-k: A 2-year randomized study. *Optom. Vis. Sci.* **2013**, *90*, 530–539. [CrossRef]

7. Lin, W.; Li, N.; Lu, K.; Li, Z.; Zhuo, X.; Wei, R. The relationship between baseline axial length and axial elongation in myopic children undergoing orthokeratology. *Ophthalmic Physiol. Opt.* **2023**, *43*, 122–131. [CrossRef]
8. Lam, C.S.Y.; Tang, W.C.; Tse, D.Y.-Y.; Lee, R.P.K.; Chun, R.K.M.; Hasegawa, K.; Qi, H.; Hatanaka, T.; To, C.H. Defocus incorporated multiple segments (DIMS) spectacle lenses slow myopia progression: A 2-year randomised clinical trial. *Br. J. Ophthalmol.* **2020**, *104*, 363–368. [CrossRef]
9. Bao, J.; Huang, Y.; Li, X.; Yang, A.; Zhou, F.; Wu, J.; Wang, C.; Li, Y.; Lim, E.W.; Spiegel, D.P.; et al. Spectacle Lenses with Aspherical Lenslets for Myopia Control vs. Single-Vision Spectacle Lenses: A Randomized Clinical Trial. *JAMA Ophthalmol.* **2022**, *140*, 472–478. [CrossRef]
10. Bao, J.; Yang, A.; Huang, Y.; Li, X.; Pan, Y.; Ding, C.; Lim, E.W.; Zheng, J.; Spiegel, D.P.; Drobe, B.; et al. One-year myopia control efficacy of spectacle lenses with aspherical lenslets. *Br. J. Ophthalmol.* **2022**, *106*, 1171–1176. [CrossRef]
11. Rappon, J.; Chung, C.; Young, G.; Hunt, C.; Neitz, J.; Neitz, M.; Chalberg, T. Control of myopia using diffusion optics spectacle lenses: 12-month results of a randomised controlled, efficacy and safety study (CYPRESS). *Br. J. Ophthalmol.* **2023**, *107*, 1709–1715. [CrossRef]
12. Gawne, T.J.; Khanal, S.; Norton, T.T. An Alternative Mechanism for the Anti-Myopia Effectiveness of Diffusion Optics Technology (DOT) Lenses. *Transl. Vis. Sci. Technol.* **2025**, *14*, 15. [CrossRef] [PubMed]
13. Swiatczak, B.; Scholl, H.P.N.; Schaeffel, F. Retinal "sweet spot" for myopia treatment. *Sci. Rep.* **2024**, *14*, 26773. [CrossRef] [PubMed]
14. Schmid, K.L.; Wildsoe, C.F. Contrast and spatial-frequency requirements for emmetropization in chicks. *Vis. Res.* **1997**, *37*, 2011–2021. [CrossRef] [PubMed]
15. Neitz, J.; Neitz, M. Diffusion optics technology (DOT): A myopia control spectacle lens based on contrast theory. *Transl. Vis. Sci. Technol.* **2024**, *13*, 42. [CrossRef]
16. Pérez, G.M.; Archer, S.M.; Artal, P. Optical characterization of Bangerter foils. *Investig. Ophthalmol. Vis. Sci.* **2010**, *51*, 609–613. [CrossRef]
17. Zhang, P.; Wang, H.; Ren, W.; Guo, H.; Yang, J.; Tao, J.; Yang, Z.; Li, Y.; Chen, L.; Zhang, Y.; et al. The Effect of Bangerter Filters on Visual Acuity and Contrast Sensitivity with External Noise. *Front. Neurosci.* **2022**, *16*, 804576. [CrossRef]
18. Jiang, J.; Zhao, T.; Yin, Y.; Han, M.; Wu, X.; Chen, Y. Bangerter filter's role in regulating ocular axial length: A novel application of an established therapy. *Eur. J. Med. Res.* **2025**, *30*, 631. [CrossRef]
19. Arias, A.; Clement, S.P.; Artal, P.; Wahl, S. Chromatic imaging properties of myopia control spectacle lenses. *Biomed. Opt. Express* **2025**, *16*, 1499–1512. [CrossRef]
20. Arias, A.; Ohlendorf, A.; Artal, P.; Wahl, S. In-depth optical characterization of spectacle lenses for myopia progression management. *Optica* **2023**, *10*, 594–603. [CrossRef]
21. Gantes-Nuñez, F.J.; Meyer, D.; Richards, J.; Aboualizadeh, E.; Kollbaum, P.S. Optical characterization of a diffusion optics technology ophthalmic lens designed for myopia control. *Investig. Ophthalmol. Vis. Sci.* **2023**, *64*, 4942.
22. Radhakrishnan, H.; Lam, C.S.Y.; Charman, W.N. Multiple segment spectacle lenses for myopia control. Part 2: Impact on myopia progression. *Ophthalmic Physiol. Opt.* **2023**, *43*, 1137–1144. [CrossRef]
23. Odell, N.V.; Leske, D.A.; Hatt, S.R.; Adams, W.E.; Holmes, J.M. The effect of Bangerter filters on optotype acuity, Vernier acuity, and contrast sensitivity. *J. Am. Assoc. Pediatr. Ophthalmol. Strabismus* **2008**, *12*, 555–559. [CrossRef]
24. Smith, E.L., III; Hung, L.-F. Form-deprivation myopia in monkeys is a graded phenomenon. *Vis. Res.* **2000**, *40*, 371–381. [CrossRef]
25. Teoh, S.C.; Collins, M.J.; Read, S.A. The short-term effect of diffuse and defocus blur on axial length and vision. *Investig. Ophthalmol. Vis. Sci.* **2020**, *61*, 2698.
26. Tran, N.; Chiu, S.; Tian, Y.; Wildsoet, C.F. The significance of retinal image contrast and spatial frequency composition for eye growth modulation in young chicks. *Vis. Res.* **2008**, *48*, 1655–1662. [CrossRef]